Electronic Supplementary Material (ESI) for Journal of Materials Chemistry C.

Opening of large band gap in metallic carbon nanotubes by mannose functionalized dendrimers: Experiments and theory

K. S. Vasu[a*], Debabrata Pramanik[a], Sudipta Kundu[a], Sridevi S[b], N. Jayaraman[c], Manish Jain[a], Prabal K. Maiti[a] and A. K. Sood[a]

[a]Department of Physics, Indian Institute of Science, Bangalore-560012, India.

[b]Department of Instrumentation and Applied Physics, Indian Institute of Science, Bangalore-560012, India.

[c]Department of Organic Chemistry, Indian Institute of Science, Bangalore-560012, India.

*Email - vasusiddeswara.kalangi@manchester.ac.uk

Computational Details:

We performed all atom MD simulations for SWNT and G4 DM along with water molecules at room temperature (T = 300 K) to get an equilibrium configuration of the composite structures. The AMBER14 software packages[1] were used for MD simulations with General Amber force field (GAFF)[2] to describe the intra and inter-molecular interactions. During 30 ns long MD simulations, DM molecule wraps around the SWNT surface to form composite structure, similar to SWNT-dendrimer structure for PETIM and PAMAM dendrimers[3,4]. This adsorption of dendrimer onto the SWNT surface produces a strain in the SWNT. Taking a portion of this strained SWNT (containing 5 unit cells along the tube axis), we calculate the electronic density of states (DOS) using density functional theory (DFT) as implemented in the Quantum Espresso software packages[5]. Periodic boundary conditions were used along nanotube axis to mimic infinite tube in DFT. Ultrasoft Pseudopotentials[6] were used to describe the electron-ion interactions. We used Perdew-Burke-Ernzerhof (PBE) approximation[7] to the exchange correlation functional. The wave functions (charge density) were expanded using plane waves[8] up to energy of 30 Ry (300 Ry). A 1x1x10 Monkhorst Pack k-point[9] sampling of the Brillouin zone with 0.005 Ry Fermi Dirac smearing, was used for self-consistent calculations. The k-grid was increased to 1×1×30 for DOS calculation. To calculate the quasiparticle band gap in semiconducting CNTs, we performed GW calculations using Berkeley GW software package[10]. Norm-conserving pseudopotentials with PBE[7] exchange-correlation functional was used to calculate the mean-field wave-functions required for the GW calculations. The dielectric matrix was expanded in plane wave with energy up to 8 Ry, and was extended to finite frequency using generalized Plasmon pole (GPP) model[11]. The number of unoccupied bands used was 5 times occupied bands and 1×1×6 k-grid was used for the GW calculations.

RBM of metallic SWNTs with different laser excitations:

The electronic transition energies (E_{ii}) are different for single walled carbon nanotubes (SWNTs) of different diameters. We have now recorded the radial breathing mode (RBM) of our metallic SWNTs samples with different laser excitations i.e. 532 nm, 633 nm and 660 nm. As shown in Fig. S2, RBM obtained with all three excitations has shown a high intensity band centered at 171 (±1) cm^{-1}, which corresponds to the diameter value of 1.45 (±0.01) nm. Besides this band, the RBM obtained with 660 nm excitation exhibited a moderately high intensity band centered at 161.1 cm^{-1} (corresponds to a diameter of 1.55 nm) and the RBM from 633 nm excitation has shown other low intensity bands centered at 153.2, 187.4 and 196.7 cm^{-1} (correspond to the diameter values of 1.63, 1.32 and 1.25 nm, respectively). Based on these observations, we confirm that our samples predominantly contain the SWNTs of diameter of ~ 1.45 nm with a partly contribution from the SWNTs of diameter of ~ 1.55 nm and a negligible contribution from the SWNTs of diameter of ~ 1.25 nm, 1.32 nm and 1.63 nm. Thus, one can envisage that the band gap opening discussed in this publication, will perhaps be feasible for the SWNTs of diameters between 1.4 to 1.6 nm.

First and second order Raman spectrum of metallic SWNTs:

Fig. S3a shows the Raman spectrum of metallic SWNTs over a broad phonon frequency range displaying typical D-band, G-band and G′-band (also known as 2D) along with weak double resonance features such as M-band and iTOLA mode[12,13]. The G-band is fitted with two components (Fig. S3b), namely, one Breit-Wigner-Fano (BWF) component (G^-) at 1542 cm^{-1} and one Lorentzian component (G^+) at 1584 cm^{-1}. The broad BWF line shape (FWHM ~ 68 cm^{-1}) of G^- component originates from phonon-plasmon coupling, is a characteristic Raman feature of metallic SWNTs[14,15]. Depending on SWNT's diameter, the broadening of both tangential components significantly increases in a certain range of laser excitation energy (E_L)

due to renormalization effects associated with the enhanced coupling between the phonons and conduction electrons[12,16]. For the metallic SWNTs of diameter ~ 1.4 nm (similar to the present case), this range is found to be $1.7 \leq E_L \leq 2.2$ eV with the effect being more prominent at $E_L \sim 2$ eV. The intensity of D-band is also known to increases in this resonance E_L range, without any significant changes in peak position[17,18]. The G′-band and its Lorentzian line shape (inset of Fig. S3b) shows the typical peak position (~ 2622 cm^{-1}) and linewidth (~ 40 cm^{-1}) of metallic SWNTs of diameter ~ 1.4 nm under 633 nm laser excitation. Further, the ratio of integrated areas of G- and D-bands (I_G/I_D) calculated from Fig. S3b is found to be ~ 15, which clearly suggest the high-purity of our metallic SWNT samples[19,20]. However, the minimal surfactant contamination in metallic SWNT samples which is difficult to be removed completely (even after multiple methanol/water washing steps for 30 mins), could also contribute to a small increase in broadening.

Band structure of metallic SWNTs and DM wrapped metallic SWNT:

SWNT wrapped with DM molecule is taken to be periodic along the axial direction. As a result, the band structure is plotted only along the axial direction. In Fig. S8, we show the DFT band structure of pristine SWNT and DM wrapped SWNT (whereas Fig. 3c in the main manuscript shows band structure of pristine unit cell of SWNT). Although the bands look symmetric around the Fermi level, there is a significant rearrangement of the bands away from the Fermi level. Furthermore, several band degeneracies are lifted in the distorted nanotube.

Bader charge analysis:

In order to show that there is no charge transfer between the SWNT and DM, Bader charge analysis for the SWNT and DM composite has been performed (shown in Fig. S9). The quantitative value of the charge transferred between DM and SWNT is 0.0083 a.u. from the Bader charge analysis—indicating that there is no significant charge transfer.

PDOS calculations and Fat band analysis:

We have now performed PDOS calculations for the both pristine and distorted (18,0) SWNT. The contribution from the p-orbitals oriented along axial direction of the tube (p_z), radial direction of atoms (p_r) and circumferential direction of atoms (p_φ) to the DOS are calculated separately. Fig. S10(a) and (b) show PDOS plot for pristine and distorted tube respectively. We can see that only p_r (π orbital of the carbon atoms) contributes near the Fermi energy of the pristine and VBM of the distorted tube.

We have also performed the fat band analysis for the pristine and distorted tubes (Fig. S11a and S11b). The bands near the Fermi energy of the pristine tube or VBM of the distorted tube are of p_r characteristic which is consistent with the PDOS calculation.

Thus from PDOS and the fat band analysis, it can be concluded that the band characteristic near the VBM of the distorted tube does not change when the tube is wrapped with DM.

Back gate transfer characteristics:

Fig. S12 illustrates the back gating characteristics of field effect transistor (FET) devices made of pristine metallic SWNTs (red color line) and metallic SWNTs functionalized with PETIM dendrimer molecules (black color line). It is clear that the behavior of gating characteristics of the FET device made of metallic SWNTs functionalized with PETIM dendrimer is similar to that of the FET device made of pristine metallic SWNTs. This confirms the absence of metal to semiconductor transition in metallic SWNTs functionalized with PETIM dendrimer molecules and hence PETIM dendrimer without mannose functionalization does not induce band gap opening in SWNTs. Thus, we are justified in confirming the observed band gap opening cannot be generalized for every dendrimer or DNA like supramolecules.

References:

1. D. A. Pearlman, D. A. Case, J. W. Caldwell, S. W. Ross, T. E. Cheatham III, S. DeBolt, D. Ferguson, G. Seibel and P. Kollman, *Comput. Phys. Commun.*, 1995, **91**, 1.
2. J. Wang, R. M. Wolf, J. W. Caldwell, P. A. Kollman and D. A. Case, *J. Compt. Chem*, 2004, **25**, 1157.
3. V. Vasumathi, D. Pramanik, A. K. Sood and P. K. Maiti, *Soft Matter*, 2013, **9**, 1372.
4. D. Pramanik and P. K. Maiti, *Soft Matter*, 2016, **12**, 8512.
5. P. Giannozzi, S. Baroni, N. Bonini, M. Calandra, R. Car, C. Cavazzoni, D. Ceresoli, G. L. Chiarotti, M. Cococcioni, I. Dabo, D. C. Andrea, S. D. Gironcoli, S. Fabris, G. Fratesi, R. Gebauer, U. Gerstmann, C. Gougoussis, A. Kokalj, M. Lazzeri, L. Martin-Samos, N. Marzari, F. Mauri, R. Mazzarello, S. Paolini, A. Pasquarello, L. Paulatto, C. Sbraccia, S. Scandolo, G. Sclauzero, A. P. Seitsonen, A. Smogunov, P. Umari and R. M. Wentzcovitch, *J. Phys.: Cond. Matt.*, 2009, **21**, 395502.
6. K. F. Garrity, J. W. Bennett, K. M. Rabe and D. Vanderbilt, *Comput. Mater. Sci.*, 2014, **81**, 446.
7. J. P. Perdew, K. Burke and M. Ernzerhof, *Phys. Rev. Lett.*, 1996, **77**, 3865.
8. G. Kresse and J. Furthmller, *Comput. Mater. Sci.*, 1996, **6**, 15.
9. H. J. Monkhorst and J. D. Pack, *Phys. Rev. B*, 1976, **13**, 5188.
10. J. Deslippe, G. Samsonidze, D. A. Strubbe, M. Jain, M. L. Cohen and S. G. Louie, *Comput. Phys. Commun.*, 2012, **183**, 1269.
11. M. S. Hybertsen and S. G. Louie, *Phys. Rev. B*, 1986, **34**, 5390.
12. S. D. M. Brown, P. Corio, A. Marucci, M. S. Dresselhaus, M. A. Pimenta, K. Kneipp, *Phys. Rev. B*, 2000, **61**, R5137.
13. P. Corio, P. S. Santos, V. W. Brar, Ge. G. Samsonidze, S. G. Chou, M. S. Dresselhaus, *Chem. Phys. Lett.* 2003, **370,** 675.
14. H. Kataura, Y. Kumazawa, Y. Maniwa, I. Umezu, S. Suzuki, Y. Ohtsuka, Y. Achiba, *Synth. Met.* 1999, **103**, 2555.
15. S. D. M. Brown, A. Jorio, P. Corio, M. S. Dresselhaus, G. Dresselhaus, R. Saito, K. Kneipp, *Phys. Rev. B* 2001, **63**, 155414.
16. M. A. Pimenta, A. Marucci, S. A. Empedocles, M. G. Bawendi, E. B. Hanlon, A. M. Rao, P. C. Eklund, R. E. Smalley, G. Dresselhaus, M. S. Dresselhaus, *Phys. Rev. B*, 1998, **58**, R16016.
17. M. A. Pimenta, E. B. Hanlon, A. Marucci, P. Corio, S. D. M. Brown, S. A. Empedocles, M. G. Bawendi, G. Dresselhaus, M. S. Dresselhaus, *Braz. J. Phys.* 2000, **30**, 423.
18. S. D. M. Brown, A. Jorio, M. S. Dresselhaus, G. Dresselhaus, *Phys. Rev. B*, 2001, **64**, 073403.
19. A. C. Dillon, T. Gennett, K. M. Jones, J. L. Alleman, P. A. Parilla, M. J. Heben, *Adv. Mater.* 1999, **11**, 1354.
20. M. E. Itkis, D. E. Perea, R. Jung, S. Niyogi, R. C. Haddon, *J. Am. Chem. Soc.* 2005, **127**, 3439.

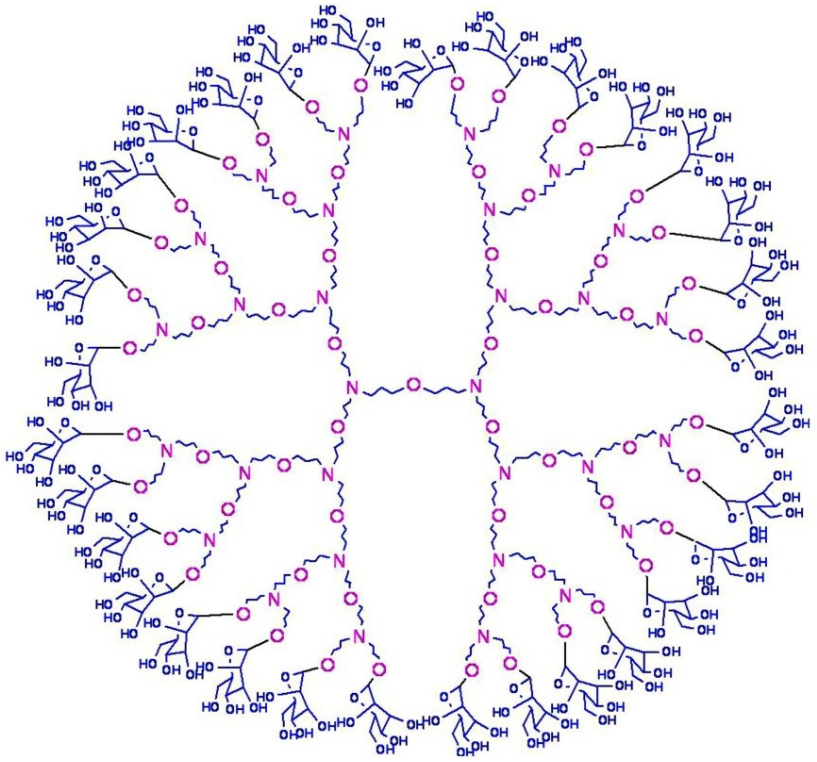

Figure S1: Chemical structure of mannose attached PETIM dendrimer.

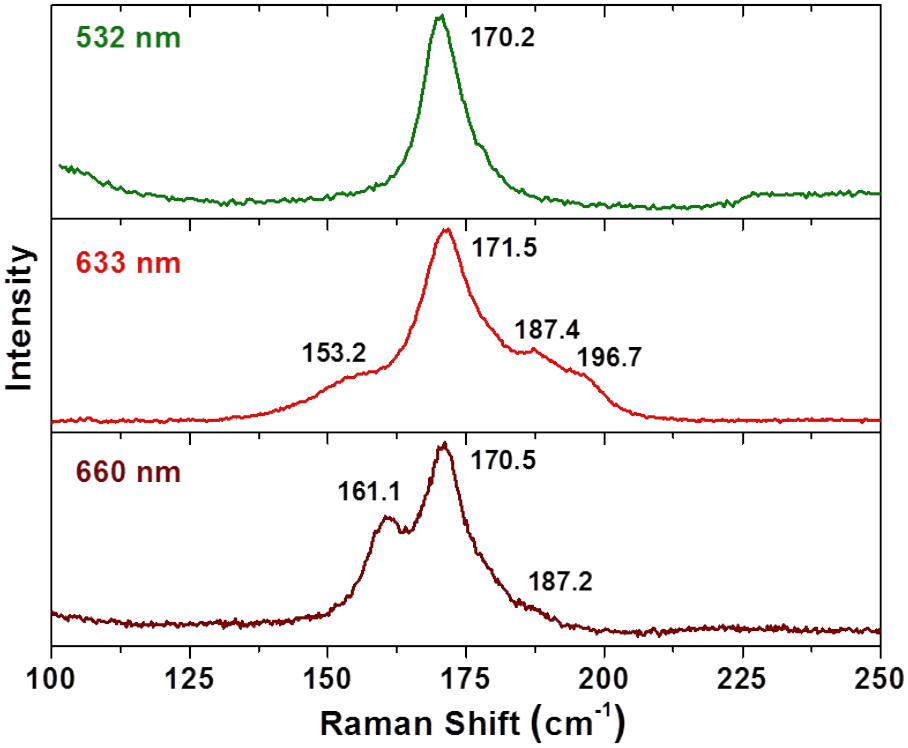

Figure S2: Radial breathing mode (RBM) of metallic SWNT samples with 532, 633 and 660 nm excitations.

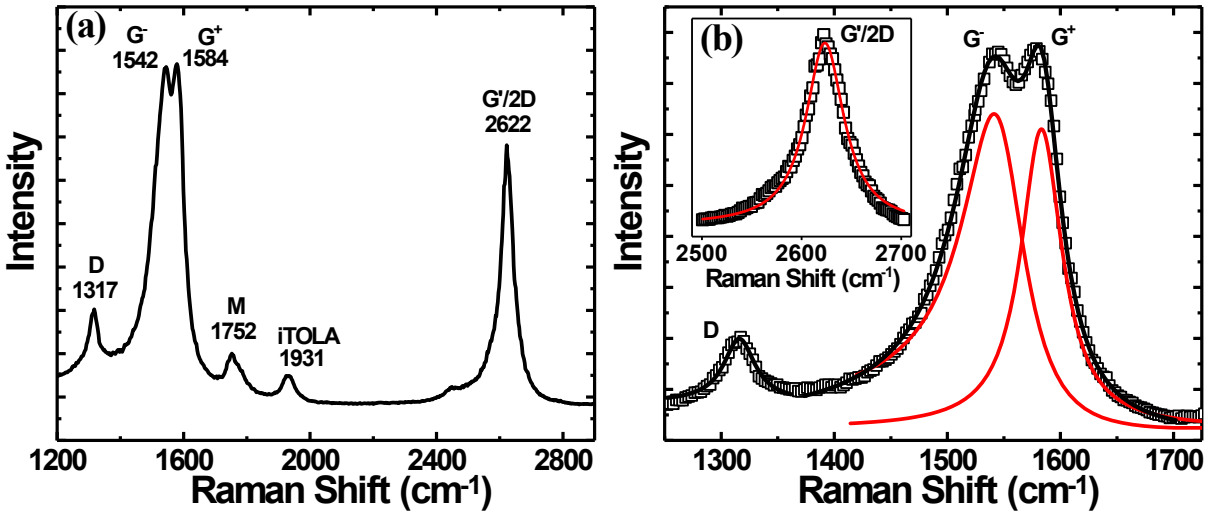

Figure S3: (a) First- and second-order Raman spectrum of metallic SWNTs over a broad range 1200-2900 cm^{-1} for 633 nm excitation. (b) Magnified display of D-, G-band and G′/2D- band (inset) of metallic SWNTs recorded using 633 nm excitation. The open squares show raw Raman data and the lines are fitted curves.

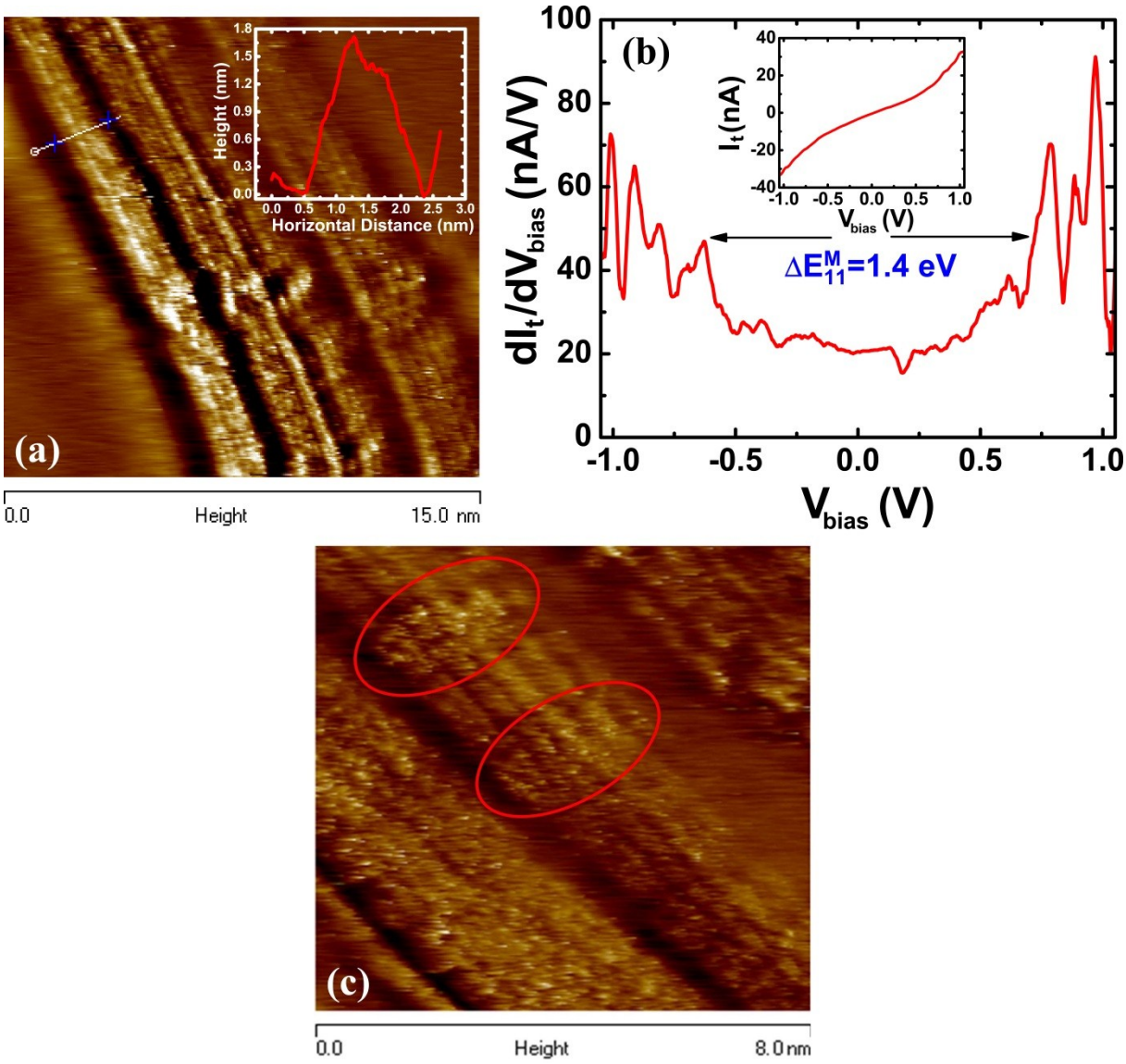

Figure S4: (a) Topographical image of metallic SWNTs (Inset: Height profile of metallic SWNTs). (b) Local dynamic tunnelling conductance as a function of bias voltage for metallic SWNT (Inset: tunnelling current as a function of V_{bias}). (c) High magnification topographical image of SWNT-DM complex on HOPG.

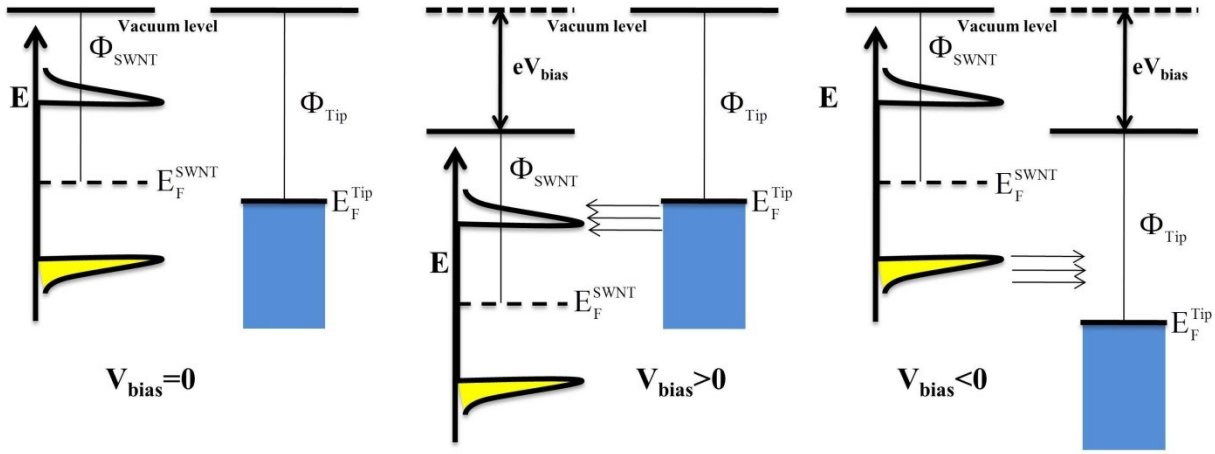

Figure S5: Energy level diagram explaining the electron transfer at V_{bias} = 0, positive and negative.

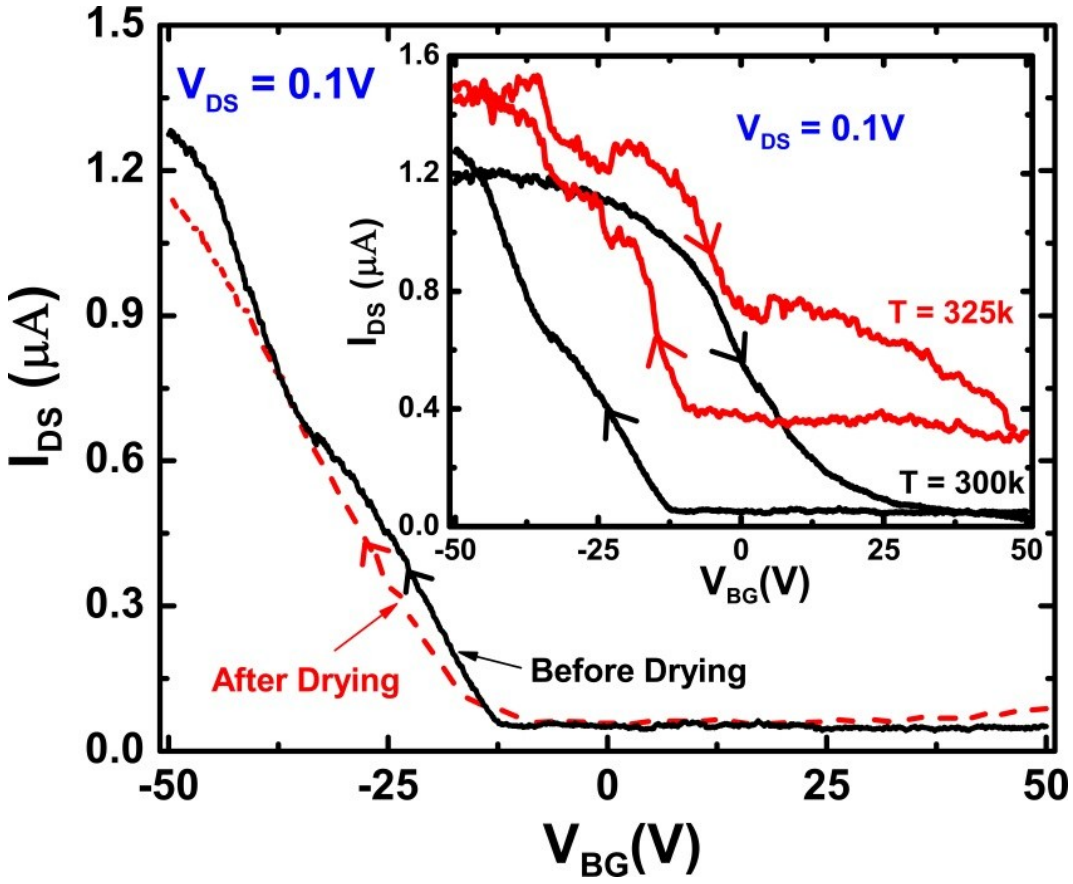

Figure S6: I_{DS}-V_{BG} characteristics of another device made of SWNT-DM complex before (black colour solid line) and after (red colour dashed line) drying in vacuum and Inset shows I_{DS}-V_{BG} characteristics of the same device at 300k and 325k.

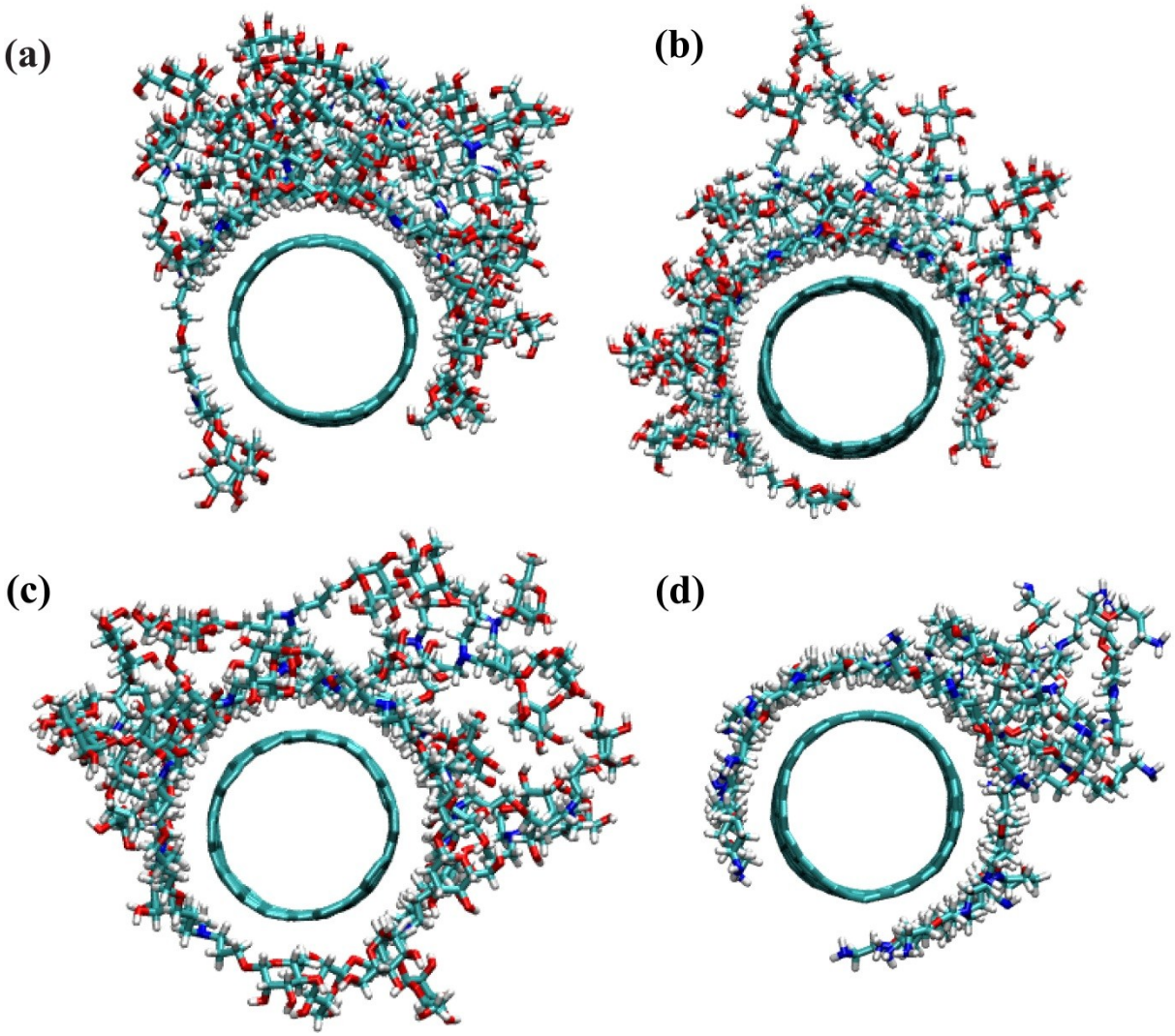

Figure S7: Instantaneous snapshots of equilibrium composite structures of dendrimer-NT after 30 ns of long MD simulations. Here the snapshots are of (a) (18,0) SWNT-DM (b) (12,9) SWNT-DM (C) (10,10) SWNT-DM and (d) (18,0) SWNT-PETIM. For clarity water molecules are not shown.

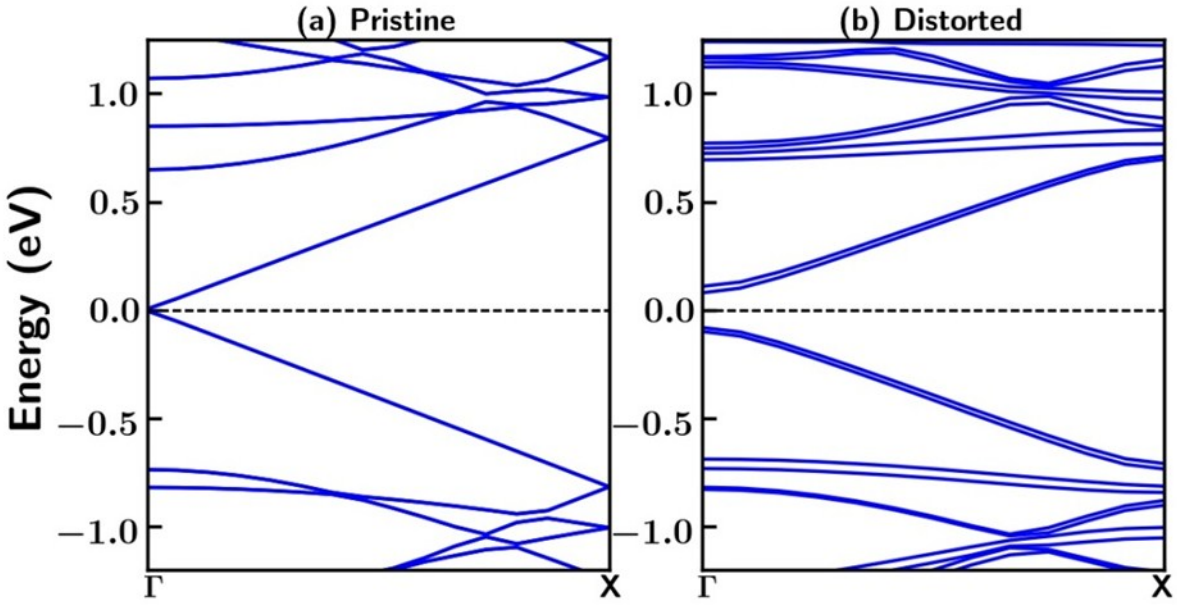

Figure S8: Band structure of the pristine (18,0) nanotube (5 unit cells along the nanotube axis) and corresponding DM wrapped nanotube. The bands are plotted along the nanotube axis.

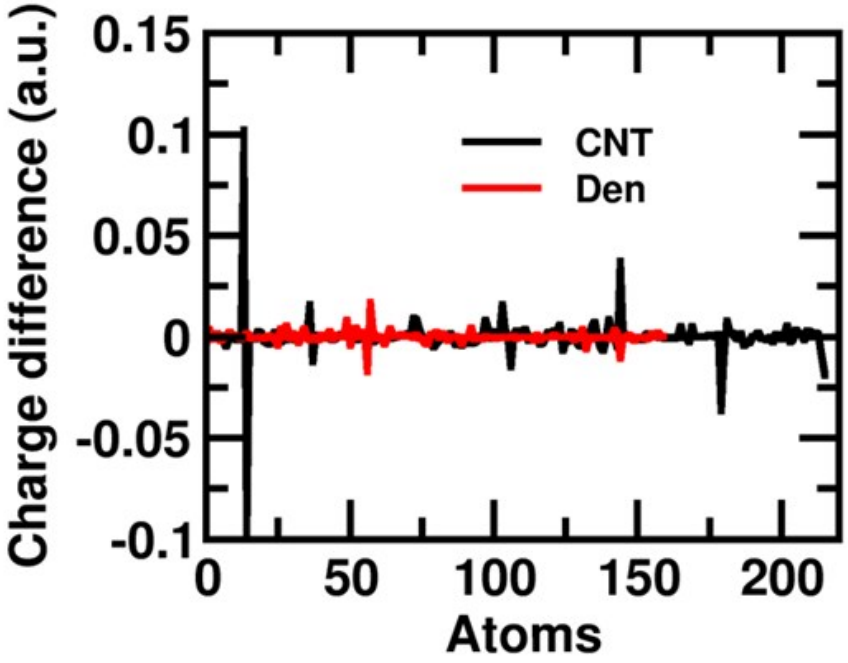

Figure S9: Bader charge analysis for SWNT and DM composite system. Charge difference between the isolated SWNT and SWNT of the composite is shown in black, whereas DM in red.

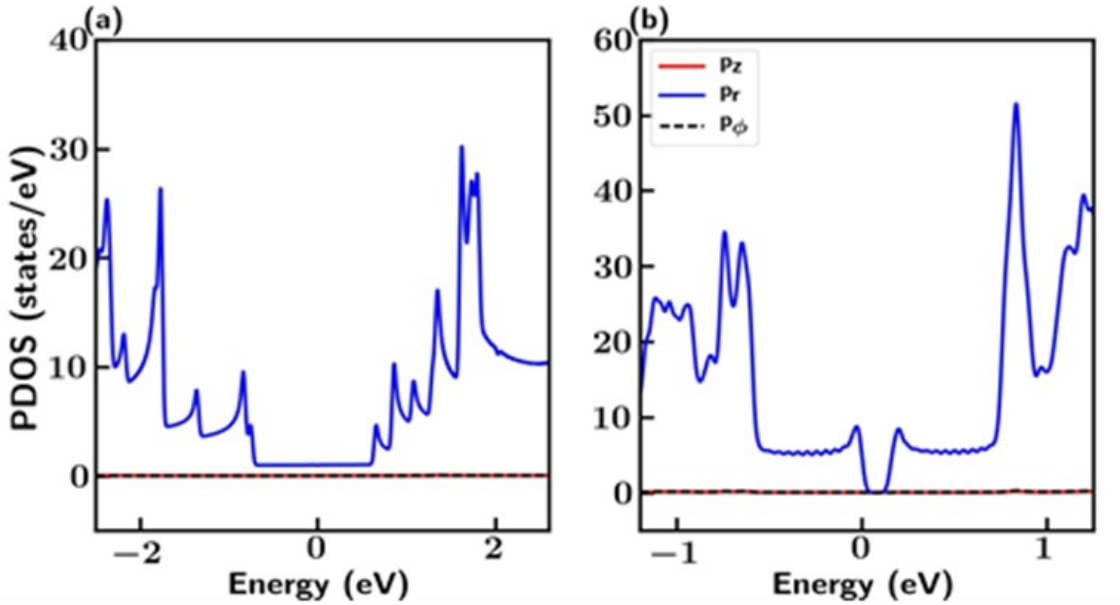

Figure S10: (a) and (b) shows PDOS for pristine and distorted tube respectively. The blue line shows the contribution from the p_r orbitals and the red and black dotted line show the PDOS due to p_z and p_{φ}. The zeros of x-axis are set to the Fermi energy for pristine and to VBM for distorted one.

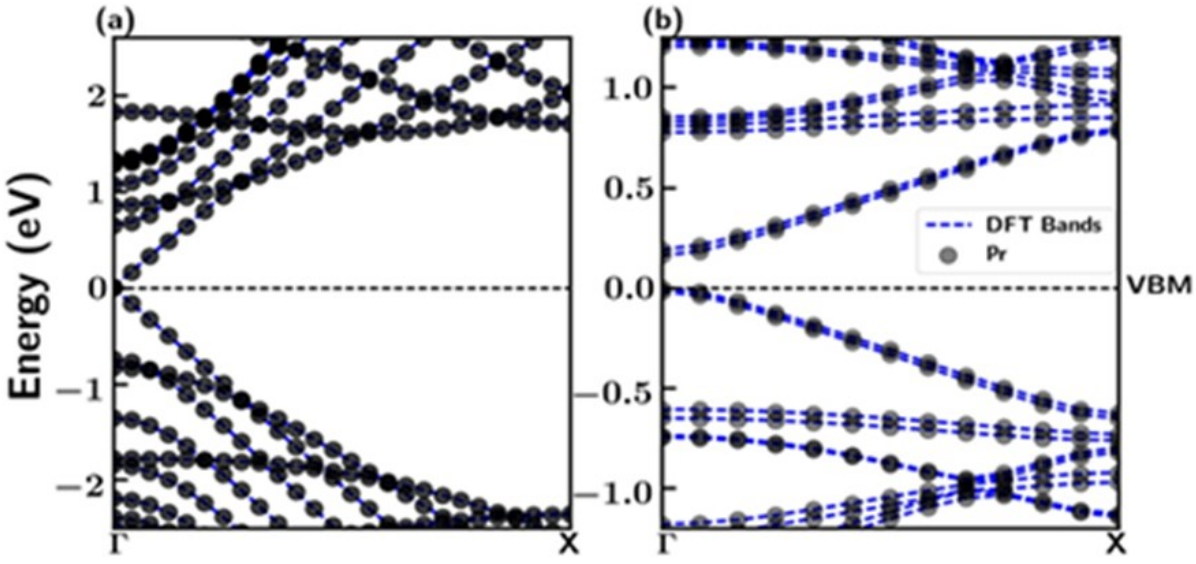

Figure S11: (a) and (b) show fat band for pristine and distorted tubes respectively. The blue dotted lines are bands obtained from DFT and the black dots give the contribution from p_r orbital. The dots are of same size as all the bands in the energy window of the plots are totally composed of p_r orbital.

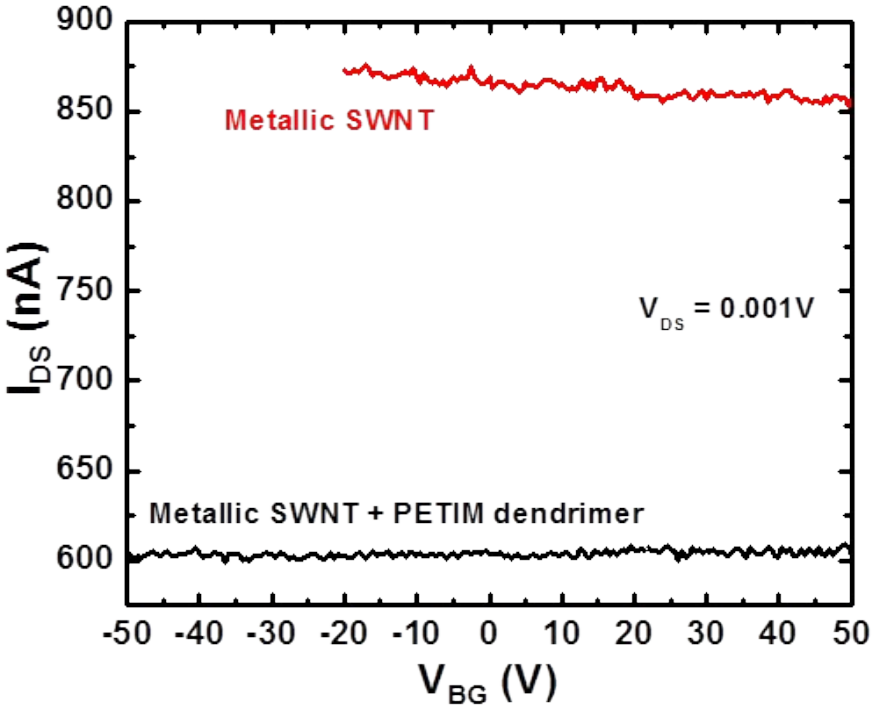

Figure S12: Back gate transfer characteristics (I_{DS} -V_{BG}) of the FET device made of metallic SWNTs before (red colour solid line) and after the complexation with PETIM dendrimer molecules (Black colour solid line).